SPECTRAL PROPERTIES OF THE TURBULENT FLOW OF A VISCOELASTIC FLUID FOR REDUCED DRAG

L. Thais
Université de Lille Nord de France, USTL
F59000 Lille, France
Laboratoire de Mécanique de Lille
CNRS, UMR 8107
F59655 Villeneuve d'Ascq, France
laurent.thais@polytech-lille.fr

T. B. Gatski
Institut Pprime
CNRS–Université de Poitiers–ENSMA
F86036 Poitiers cedex, France
Center for Coastal Physical Oceanography
Old Dominion University
Norfolk, Virginia 23529 USA
thomas.gatski@univ-poitiers.fr

G. Mompean
Université de Lille Nord de France, USTL
F59000 Lille, France
Laboratoire de Mécanique de Lille
CNRS, UMR 8107
F59655 Villeneuve d'Ascq, France
gilmar.mompean@polytech-lille.fr

ABSTRACT

In the present study, direct numerical simulation (DNS) results of fully developed turbulent channel flows of a viscoelastic fluid modeled as a polymer dilution in a Newtonian solvent are analyzed. The analysis is focused on the spectral properties of the turbulent stress and vorticity fields in order to contrast the properties of turbulence of viscoelastic and Newtonian fluids, and to quantify the effects of increased elasticity on the spectral behavior. The simulation results coupled with the spectral analysis just mentioned can be useful in further assessing the two classes of explanations that have been proposed by Lumley (1969) and De Gennes (1986) for the occurrence of polymer drag reduction.

FORMULATION

The incompressible flow field under consideration is a fully developed turbulent channel flow of a FENE-P viscoelastic fluid. The channel streamwise direction is $x_1 = x$, the wall-normal direction is $x_2 = y$, and the spanwise direction $x_3 = z$. The instantaneous velocity field is $(u, v, w) = (u_1, u_2, u_3)$, and the variables are scaled with the bulk velocity U_b and the channel half-height h. The channel is also assumed of infinite extent in the spanwise direction.

The equations governing the motion of a dilute polymer solution are the mass and momentum conservation equations closed with the constitutive equation for the viscoelastic fluid.

Mass and Momentum Conservation

With the length and time respectively scaled by $\nu_0/u_{\tau 0}$ and $\nu_0/u_{\tau 0}^2$, where ν_0 is the total (solvent+polymer) viscosity and $u_{\tau 0}$ the zero-shear friction velocity, the dimensionless conservation equations are:

$$\frac{\partial u_j^+}{\partial x_j^+} = 0 \qquad (1a)$$

$$\frac{\partial u_i^+}{\partial t^+} + u_j^+ \frac{\partial u_i^+}{\partial x_j^+} = -\frac{\partial P^+}{\partial x_i^+} + \frac{\partial \Xi_{ij}^+}{\partial x_j^+} \qquad (1b)$$

The pressure is P^+ and the stress tensor Ξ_{ij}^+ is composed of (Newtonian) solvent and (polymeric) viscoelastic contributions,

$$\Xi_{ij}^+ = 2\beta_0 s_{ij}^+ + \Xi_{ij}^{p+} \qquad (2)$$

with the strain rate tensor $s_{ij}^+ = (\partial u_i^+/\partial x_j^+ + \partial u_j^+/\partial x_i^+)/2$, β_0 the ratio of the Newtonian viscosity ν_N to the total zero-shear viscosity $\nu_0 = \nu_N + \nu_{p0}$, and $Re_{\tau 0} = u_{\tau 0} h/\nu_0$ the zero-shear friction Reynolds number. A uniform polymer concentration is assumed characterized by the viscosity ratio β_0 (the limit $\beta_0 = 1$ is a Newtonian fluid). This quantity was here fixed to $\beta_0 = 0.9$.

Constitutive Equation

The polymeric extra-stress,

$$\Xi_{ij}^{p+} = \frac{1-\beta_0}{We_{\tau 0}} \left[f(\{\mathbf{c}\}) c_{ij} - \delta_{ij} \right] \qquad (3)$$

associated with the dilute polymer solution is proportional to the polymer dilution parameter $1 - \beta_0$, inversely proportional to the friction Weissenberg number $We_{\tau 0}$ (ratio of

(a) Mean velocity
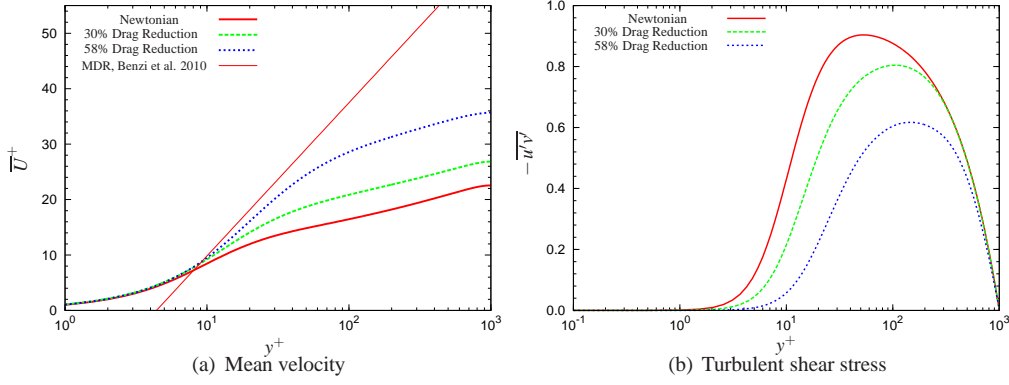

(b) Turbulent shear stress

Figure 1.   (a) Mean velocity profiles and (b) Turbulent shear stress channel across half-width for Newtonian and viscoelastic flows at frictional Reynolds number $Re_{\tau 0} = 1000$

elasticity to turbulent time scale), and is related to the conformation tensor components c_{ij}, which represent the ensemble average squared norm of the end-to-end vector of the polymer molecules. The function

$$f\left(\{\mathbf{c}\}\right) = \frac{L^2 - 3}{L^2 - \{\mathbf{c}\}} \qquad (4)$$

follows the Peterlin approximation, with L the fully-stretched polymer chain length and $\{\mathbf{c}\}$ the trace of the conformation tensor $\mathbf{c}$. The evolution equation for the conformation tensor in wall units is

$$\frac{\partial c_{ij}}{\partial t^+} + u_k^+ \frac{\partial c_{ij}}{\partial x_k^+} = \left(c_{ik}s_{kj}^+ + s_{ik}^+ c_{kj}\right) - \left(c_{ik}w_{kj}^+ - w_{ik}^+ c_{kj}\right)$$
$$+ \frac{f(\{\boldsymbol{c}\})c_{ij} - \delta_{ij}}{We_{\tau 0}} \qquad (5)$$

where $w_{ij}^+ = (\partial u_i^+/\partial x_j^+ - \partial u_j^+/\partial x_i^+)/2$ is the rotation rate tensor.

Numerical Method and Relevant Simulation Parameters

Solving the conservation and constitutive equations involves a hybrid spatial scheme with Fourier-Galerkin spectral accuracy in the two homogeneous directions and 6th-order compact finite differences for first and second-order wall-normal derivatives. In the wall-normal direction, we make usage of Hermitian (or Padé) techniques which are locally supported, and possess spectral-like approximation properties (Lele, 1992; Carpenter, 1993). A detailed description of the numerical procedure can be found in Thais *et al.* (2011). The resulting parallel algorithm is highly scalable, which allows DNS at (relatively) high Reynolds numbers in large computational boxes for both Newtonian and viscoelastic flows. Various degrees of drag reduction can be obtained at a given Reynolds number $Re_{\tau 0}$ through different choices of the maximum chain extensibility L, and friction Weissenberg number $We_{\tau 0}$. In a recent study (Thais *et al.*, 2012), the Reynolds number similarity of the flow statistics at a high drag reduction regime of the order of 60% have been probed. For the present study, the parameter set $\beta_0 = 0.9$ at a fixed Reynolds number $Re_{\tau 0} = 1000$ with two drag reduction cases are considered: $L = 30$, $We_{\tau 0} = 50$,

corresponding to a medium percentage drag reduction (DR) of 30%, and $L = 100$, $We_{\tau 0} = 115$, corresponding to a high percentage DR of 58%. The statistics and the spectral properties of these 2 flow cases are explored in contrast with the reference Newtonian flow at the same Reynolds number.

RESULTS
Flow statistics

In Fig. 1(a) is shown the effect of increased viscoelasticity on the mean velocity where the well-known thickening of the viscous sublayer is evident. Also shown in Fig. 1(a) is the asymptotic limit of maximum drag reduction (MDR) theoretically predicted by Benzi (2010), in agreement with experimental evidence by Virk (1975). One notices a steepening of the viscoelastic velocity profiles in the near-wall layer, the high drag reduction flow case getting close to the MDR asymptote in this region. Such behavior suggests a significant extension of the sublayer/buffer layer regions into the channel as viscoelasticity increases. In the outer layer, a broad log-law region appears for the intermediate viscoelastic flow, which had not been observed in previous DNS at lower Reynolds numbers, see e.g. Housiadas & Beris (2003). Correspondingly, the peak turbulent shear stress is shifted outward, and its magnitude reduced down to a third of the Newtonian value in the high drag reduction case.

The mean turbulent kinetic energy (TKE) distribution displayed in Fig. 2(a) is also shifted outward, with an increase in peak magnitude in viscoelastic flows. The simulations have shown that this increase in TKE is due solely to an increase in the streamwise normal turbulent stress component since the wall-normal and spanwise components all show a decrease relative to the Newtonian values. The nonlinear spring force of a finitely extendable nonlinear elastic (FENE) polymer model is governed by Warner's law (see for example Deville & Gatski, 2012). This force results in a mean elastic potential energy

$$E_p^+ = \frac{1}{2}\alpha_0 \left(L^2 - 3\right) \overline{\ln\left[f(\{\boldsymbol{c}\})\right]} \qquad (6)$$

where $\alpha_0 = (1 - \beta_0)/We_{\tau 0}$. As shown in Fig. 2(b), E_p^+ remains at a relatively modest fraction of the peak turbulent kinetic energy in the medium drag reduction flow, whereas it reaches about half the peak TKE value in the high drag reduction flow.
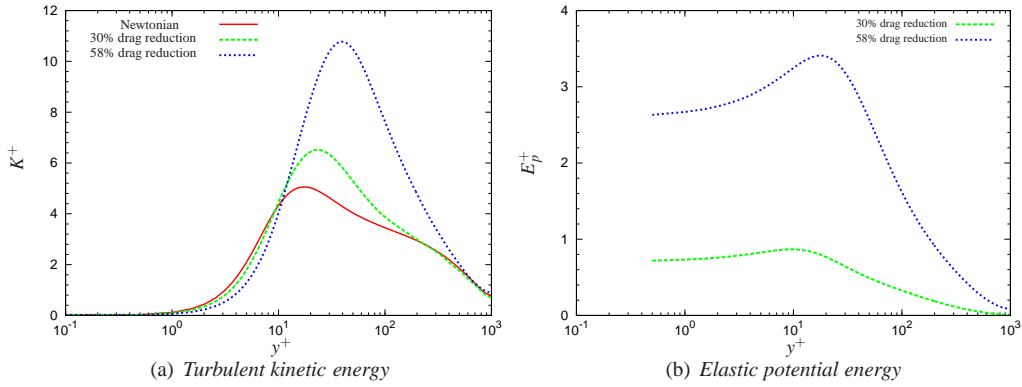
2

(a) *Turbulent kinetic energy*

(b) *Elastic potential energy*

Figure 2. *Distributions of (a) turbulent kinetic energy and (b) mean elastic potential energy across channel half-width at frictional Reynolds number $Re_{\tau 0} = 1000$*

Spectral Properties in the Inner Layer

In view of probing the velocity field power spectra, it is advantageous to exploit the Fourier-Galerkin spatial scheme used in the two homogeneous directions x and z. The discrete pre-multiplied two-dimensional (2D) power spectral density of the u_i velocity component can be straightforwardly evaluated in Fourier space through

$$\Phi_{ii}(k_x, k_z, y) = k_x k_z \langle \hat{u}_i \hat{u}_i^* \rangle \qquad (7)$$

with k_x, k_z the discrete wavenumbers in each respective direction. The quantity $\langle \hat{u}_i \hat{u}_i^* \rangle$ is the time-averaged two-dimensional power spectral density[1] of the u_i velocity component, which is here taken in wall-parallel slabs over 500 flow snapshots spanning approximately 5 eddy turnover times. From the 2D-power spectral density, it is also straightforward to evaluate the discrete 1D-power spectral densities in each direction x and z by integration in the respective orthogonal direction. Here, we shall restrict ourselves to the 1D-x power spectral density in the streamwise direction, which can be evaluated through integration in the cross-channel direction

$$E_{ii}(k_x, y) = \left(\frac{2\pi}{L_z}\right) \sum_{k_z = -\left(\frac{2\pi}{L_z}\right).N_{gz}}^{\left(\frac{2\pi}{L_z}\right).N_{gz}} \langle \hat{u}_i \hat{u}_i^* \rangle (k_x, k_z, y) , \qquad (8)$$

where L_z is the channel width, and N_{gz} the number of Fourier Galerkin modes in the same direction.

Figure 3 shows velocity and vorticity power spectral densities at the fixed position from the wall $y^+ = 99$. A marked alteration of the spectral properties in the presence of the polymer appears over the entire wavenumber range. For the 'large' scales, the k^{-1} energy spectrum hypothesis in the one-dimensional power spectrum of the streamwise velocity, first evidenced by Laufer (1955), is here confirmed for the Newtonian flow over a significant wavenumber range $5.10^{-4} \lesssim k_x \eta \lesssim 10^{-2}$ (η is the Kolmogorov viscous scale). This wavenumber range is almost unaltered in the medium drag reduction flow, whereas a clear enhancement of the low wavenumber energy is observed in the high drag reduction flow. In the mean time, the k^{-1} wavenumber range in the high drag reduction flow, if any, is considerably narrower.

However, the most striking property in Fig. 3 is the pronounced drop of energy in all three components in the high wavenumber range as viscoelasticity increases. In the high drag reduction case, there is a clear tendency towards a k_x^{-5} power law over a full decade in the wavenumber range $10^{-2} \lesssim k_x \eta \lesssim 10^{-1}$ for the streamwise and spanwise velocity spectral densities. This observation is in line, at least qualitatively, with the experimental data of Warholic *et al.* (1999). In particular, their figure 15 shows a similar dramatic drop in the energy density function of the streamwise velocity component. Although their plot is a frequency spectrum, one can extrapolate, using the Taylor frozen-turbulence hypothesis, a power law region approximately following k_x^{-4} to k_x^{-5} for their 3 high drag reduction flow cases (55%, 64% and 69% percent drag reduction). One should also notice that the wall-normal velocity spectrum exhibits a singular behavior. The wall-normal low wavenumber range shows no energy enhancement for the two viscoelastic flows. In contrast, the high wavenumber decay rate is slower than in the other two directions, following a $O(k_x^{-4})$ decay rate.

The 1D-power spectral densities of the 3 components of vorticity at the same wall-normal position $y^+ = 99$ are plotted in Fig. 4. For the spectra of the streamwise component of vorticity, one finds a similar behavior to the spectra of the wall-normal velocity component (Fig. 3(c)). The large scales are little affected by viscoelasticity; whereas, viscoelasticity induces a drop in the energy content following a k_x^{-3} power law from the middle of the inertial subrange, $k_x \eta \gtrsim 10^{-2}$, down to the smallest resolved scales. The spectra of the other two components of vorticity have a distinct behavior. The spectra of the spanwise and wall-normal vorticity components in the viscoelastic cases cross the Newtonian spectra around $k_x \eta \approx 10^{-2}$; the crossing wavenumber being slightly smaller at high drag reduction, which is similar to the results obtained for the velocity spectra. One will also notice the existence of a steeper drop following a power law k_x^{-4} in the inertial subrange. Viscoelasticity effects are most noticeable in the cross-stream component of vorticity (Fig. 4(b)). For this component, the large scale energy content is increased by more than an order of magnitude in the high drag reduction flow with respect to

---

[1] $\langle \hat{u}_i \hat{u}_i^* \rangle$ is time-averaged power per unit spectral ray, or time-averaged power spectral density, the overhat standing for the unscaled 2D-discrete Fourier transform coefficients. The star is complex conjugation, and the angle brackets are for time-averaging.

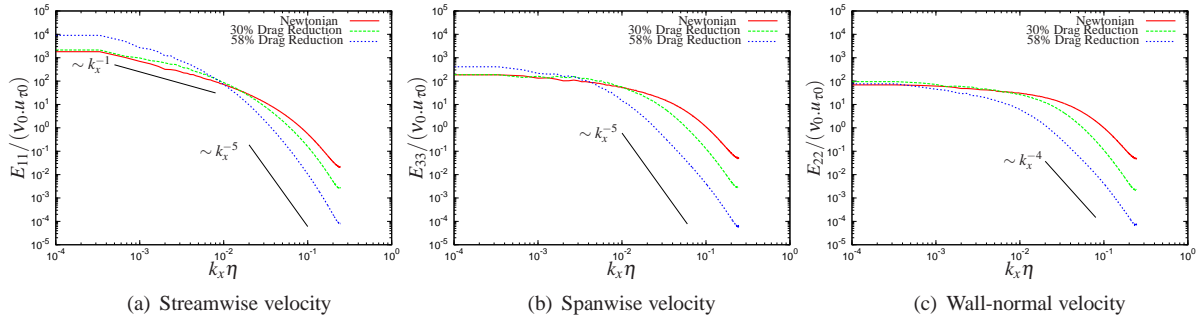| (a) Streamwise velocity | (b) Spanwise velocity | (c) Wall-normal velocity |

Figure 3. 1D-power spectral density of (a) the streamwise velocity, (b) the spanwise velocity and (c) the wall-normal velocity component at the wall-normal position $y^+ = 99$ for Newtonian and viscoelastic flows at $Re_{\tau 0} = 1000$. η is the Kolmogorov viscous scale based on the zero-shear total viscosity.

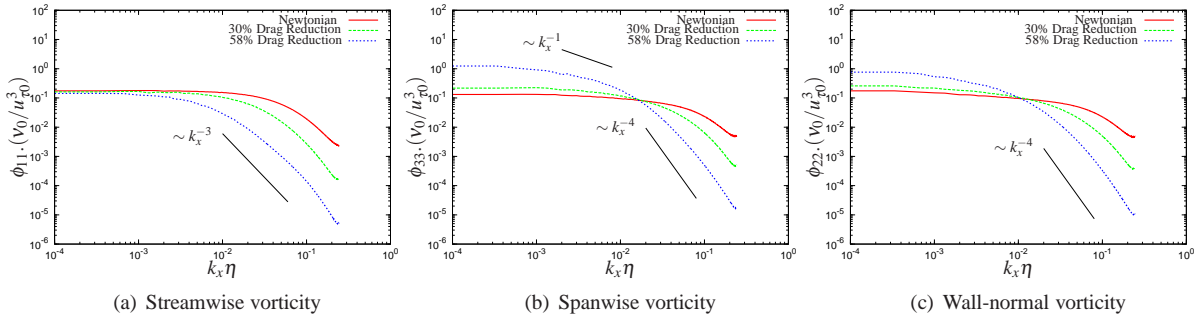| (a) Streamwise vorticity | (b) Spanwise vorticity | (c) Wall-normal vorticity |

Figure 4. 1D-power spectral density of the 3 components of vorticity $\phi_{ii}^+ = \phi_{ii} \cdot (\nu_0 / u_{\tau 0}^3)$ at the wall-normal position $y^+ = 99$ for Newtonian and viscoelastic flows at $Re_{\tau 0} = 1000$.

the Newtonian flow. Also, there is a tendency towards a k_x^{-1} behavior for the high drag reduction flow in the low wavenumber range $2.10^{-3} \lesssim k_x \eta \lesssim 8.10^{-3}$. This result is in line with the findings of Morris & Foss (2005) who reported large values of the spectral density of the cross-flow vorticity at the low and inertial ranges of wavenumbers in inhomogeneous high Reynolds number Newtonian turbulent flow. This suggests that such a decay law in the viscoelastic case is a result of the increased anisotropy level. Another feature of the heightened anisotropy of these flows is the existence of power laws in the vorticity spectra at high wavenumbers. In homogeneous, isotropic turbulence no such power law appears in the inertial subrange (Pope, 2000).

Spectral Properties at the Channel Mid-Plane

Many properties of our data plead in favor of Lumley's "effective" viscosity theory: the extension of the sublayer into the channel, the relaxation of the TKE profiles towards the Newtonian values in the outer layer, the fact that the MDR asymptote can be predicted with an extensional viscosity hypothesis (Benzi, 2010), etc. However, Lumley's theory essentially follows (modified) boundary layer arguments, i. e. the presence of a mean shear flow is an essential ingredient to the polymer alteration of momentum.

Figures 5 and 6 repeat the velocity and vorticity spectra shown above but right at the channel mid-plane. Here, the Newtonian and medium drag reduction spectra are virtually the same, indicating that the polymer has little, if any, influence on the turbulent structures outside the log-layer in the medium drag reduction flow. This would again plead in favor of Lumley's viscous theory. However, the high drag

reduction spectra again exhibit a high wavenumber energy drop, and a low wavenumber energy increase; although both effects are less pronounced than observed in the inner layer, showing that the spectra can be altered by the polymer in the absence of any mean shear. There is no tendency towards a power law drop of the energy for the spanwise and wall-normal velocity components. However, for Newtonian flow and for medium drag reduction flow, there is a discernible inertial wavenumber range where the $k^{-5/3}$ decay law applies to the streamwise spectra. In contrast, no such $k^{-5/3}$ law applies to the high drag reduction flow over a significant wavenumber range.

At the channel mid-plane, the polymer effect on turbulent structures is isotropic, in contrast with the observation in the inner layer, which is particularly conspicuous when examining the vorticity spectra in Fig. 6. In these vorticity spectra, one will also notice a small, yet non-negligible, dampening at high wavenumbers for the medium drag reduction flow case.

SPECTRAL ANALYSIS FOR HOMOGENEOUS ISOTROPIC TURBULENCE

The spectra at the channel mid-plane suggest to investigate the Fourier transformed evolution equations in the framework of homogeneous isotropic turbulence. The various 3D-Fourier transformed variables[2] are now formally written as

$$\widetilde{g}(\mathbf{k}, t) = \frac{1}{(2\pi)^3} \int g(\mathbf{x}, t) \, e^{\imath \mathbf{k} \cdot \mathbf{x}} \, d^3 \mathbf{x} \qquad (9a)$$

---

[2]The '+' sign for inner scaling is omitted from now on for conciseness
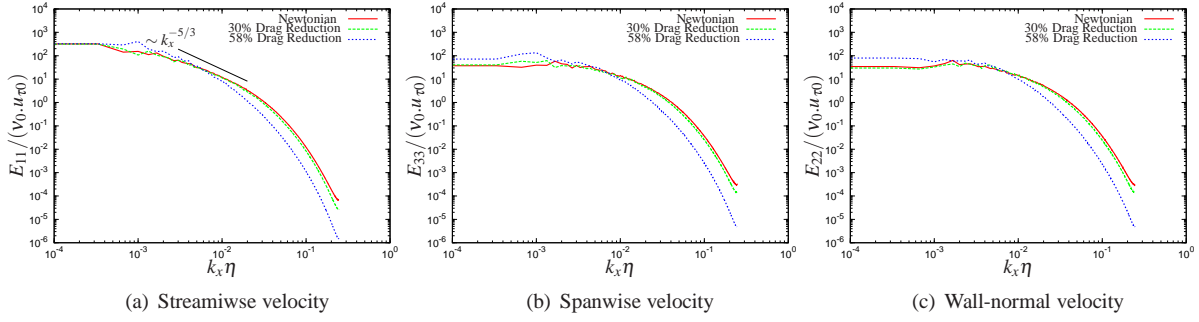
4

Figure 5. 1D-power spectral density of the 3 velocity components $E_{ii}^{+} = E_{ii}/(v_0.u_{\tau 0})$ at the mid-channel center plane for Newtonian and viscoelastic flows at $Re_{\tau 0} = 1000$. on the zero-shear total viscosity. (a) Streamwise velocity-u (b) Spanwise velocity-w (c) Wall-normal velocity-v
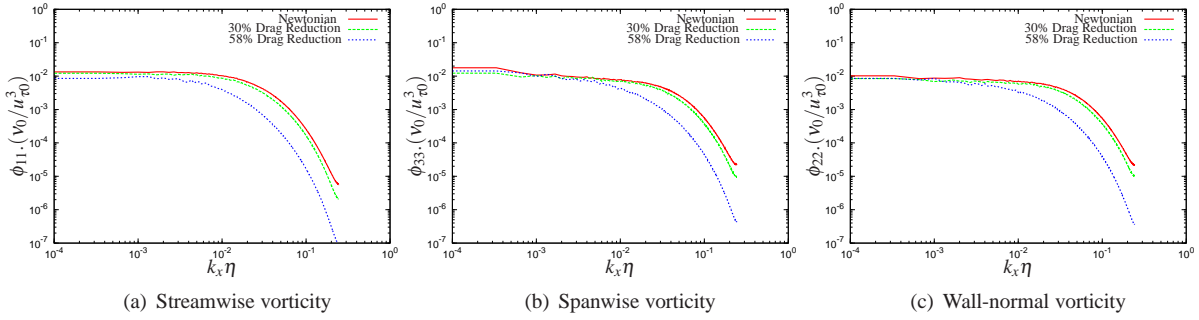

Figure 6. 1D-power spectral density of the 3 components of vorticity $\phi_{ii}^{+} = \phi_{ii}.(v_0/u_{\tau 0}^3)$ at the mid-channel center plane for Newtonian and viscoelastic flows at $Re_{\tau 0} = 1000$.

$$g(\mathbf{x},t) = \int \widetilde{g}(\mathbf{k},t)\, e^{-\iota \mathbf{k}\cdot\mathbf{x}}\, d^3\mathbf{k} \qquad (9b)$$

with $\iota = \sqrt{-1}$ and $\mathbf{k}$ the circular 3D-wavenumber vector. The respective instantaneous fluctuating Fourier transformed continuity and momentum equations are then

$$k_j \widetilde{u}_j = 0 \qquad (10a)$$

$$\frac{\partial \widetilde{u}_i}{\partial t} - \iota k_j \widetilde{u}_j \star \widetilde{u}_i = \iota k_i \widetilde{p} - \beta_0 \kappa^2 \widetilde{u}_i - \iota k_j \widetilde{\Xi}_{ij}^{p} \qquad (10b)$$

where

$$\Xi_{ij}^{p} = \alpha_0 \left[\widetilde{f} \star \widetilde{c}_{ij} - \widetilde{\delta}_{ij} \right] \qquad (11)$$

has been used for the Fourier transformed extra-stress, with $\kappa = |\mathbf{k}|$, $\widetilde{\delta}_{ij} = \delta(\mathbf{k})\delta_{ij}$, and the $\star$ standing for the Fourier convolution product. Multiplying the momentum equation by k_i, and using Eq. (10a), gives

$$\widetilde{p} = -\frac{k_i k_j}{\kappa^2} \left[\widetilde{u}_j \star \widetilde{u}_i - \widetilde{\Xi}_{ij}^{p} \right] \qquad (12)$$

Substituting back in the momentum equation yields

$$\frac{\partial \widetilde{u}_i}{\partial t} + \beta_0 \kappa^2 \widetilde{u}_i = \iota k_j \left[\delta_{il} - \frac{k_i k_l}{\kappa^2} \right] \left[\widetilde{u}_j \star \widetilde{u}_l - \widetilde{\Xi}_{jl}^{p} \right] \qquad (13)$$

A first-order time integration of Eq. (13) yields

$$\widetilde{u}_i = \widetilde{u}_i|_{t=0} + \iota k_j t \times$$

$$\left[\delta_{il} - \frac{k_i k_l}{\kappa^2} \right] \left[\widetilde{u}_j \star \widetilde{u}_l - \alpha_0 \left(\widetilde{f} \star \widetilde{c}_{jl} - \widetilde{\delta}_{jl} \right) \right]$$
$$+ \mathcal{O}\left(\kappa^2 \right) \qquad (14)$$

The second term with the $\mathcal{O}(\kappa)$ contribution consists of the usual Newtonian contribution, with an additional FENE-P contribution that has the potential to significantly contribute to the small k behavior of the velocity Fourier coefficient. When $\widetilde{u}_i|_{t=0}$ is smaller than $\mathcal{O}(\kappa)$, this entire second term dominates but with features distinct from the Newtonian behavior. Any inter-modal component transfer represented by the convolution between the Peterlin function and the conformation tensor does not involve the velocity field in this equation so that the imposed stress due to the polymer acts independent of the velocity field here. This is a fundamental effect and would carry over to flows with mean shear. As such the enhanced spectral values observed at low wavenumbers (large scales) would be due to the influence of this term. From Eq. (14), it is shown that at low wavenumber the functional behavior with respect to wavenumber is the same as the Newtonian case; just at a different magnitude level. The polymer force is proportional to the Peterlin function. As the polymer is stretched the denominator of the Peterlin function gets closer to zero (although it can never reach maximum extensibility). The polymeric term in Eqs. (13) and (14) are clearly dependent on the Peterlin function and in a nonlinear way since this is a convolution.

Thinking in a linear fashion, this term would suggest that an increase in stretching, i. e. an increase in the Peterlin function, should strengthen the polymeric effect. Figure 7 shows profiles of the Peterlin function across the channel half-width. In this figure, a linear y-scale was used to magnify the behavior towards the channel center. Not sur-
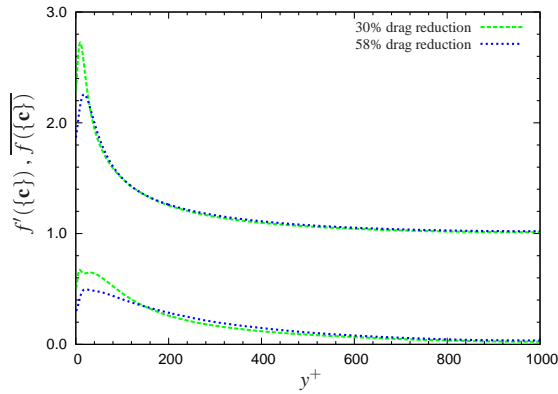
5

Figure 7. *Mean and fluctuating contributions to the Peterlin function*

prisingly, the mean contribution $\overline{f(\{\mathbf{c}\})}$ (2 top curves) relax to unity towards the channel center, while the fluctuating contribution $f'(\{\mathbf{c}\})$ (2 bottom curves) relax to zero. However, both contributors to the Peterlin function are larger in the medium drag reduction flow. Furthermore, the Fourier-transformed polymer stress $\widetilde{\Xi}_{ij}^p$ is proportional to the coefficient α_0, which is larger in the medium drag reduction ($\alpha_0 = 2 \times 10^{-3}$) than in the high drag reduction flow ($\alpha_0 = 0.9 \times 10^{-3}$). These observations come in contradiction with the above mentioned linear way of thinking. We conclude that polymer stretching cannot be responsible for the alteration of the energy cascade at the channel mid-plane, in particular the high-wavenumber attenuation cannot be explained with this argument.

This is further confirmed upon using Eq. (13) to form the evolution equation for the energy density $\Phi_{ii}(\mathbf{k}) = \int \widetilde{u_i}(\mathbf{k})\widetilde{u_i^*}(\mathbf{k'})d^3\mathbf{k'}$. After some algebra, the final result is

$$\frac{d\Phi_{ii}}{dt} + 2\beta_0 \kappa^2 \Phi_{ii} + P_p(\mathbf{k}) = T(\mathbf{k}) \qquad (15)$$

In Eq. (15), $T(\mathbf{k})$ is the usual (Newtonian) triadic conservative interchange of energy between wavenumber components (e.g. Durbin & Pettersson-Reif, 2010), whereas $P_p(\mathbf{k})$ is an additional polymeric contribution

$$P_p(\mathbf{k}) = \iota \alpha_0 k_l \int \{p_{ili}(\mathbf{k},\mathbf{p}) - p_{ili}^*(\mathbf{k},\mathbf{p})\} d^3\mathbf{p} \qquad (16)$$

where

$$p_{ili}(\mathbf{k},\mathbf{p}) = \overline{\widetilde{u_i^*}(\mathbf{k})\left[\widetilde{f}(\mathbf{k}-\mathbf{p}) \star \widetilde{c}_{il}(\mathbf{p})\right]} \qquad (17)$$

In Eq. (15), the spectral transfer term $T(\mathbf{k})$ is the same as in the Newtonian case. This means it neither adds or subtracts energy to the system and simply transfers energy, presumably from low to high wavenumbers. Once again, however, the Peterlin function is present in the polymeric term $p_{ili}(\mathbf{k},\mathbf{p})$, and it acts non-linearly through the presence of a convolution product.

Since the turbulent kinetic energy is given as $K = 1/2 \int \Phi_{ii}(\mathbf{k})d^3\mathbf{k}$, Eq. (15) translates in physical space as

$$\frac{dK}{dt} = -\varepsilon - \frac{1}{2}\int P_p(\mathbf{k}) \, d^3\mathbf{k} \qquad (18)$$

where $\varepsilon = \beta_0 \int k_l k_l \Phi_{ii}(\mathbf{k}) \, d^3\mathbf{k}$ is the solenoidal dissipation rate of TKE. It appears that even if the turbulence field is isotropic the decay of TKE is affected by the polymeric contribution. This suggests that the Kolmogorov cascade can be altered across a broad spectral range.

The right side of Eq. (18) shows the complicated interaction between the viscous dissipation rate and the polymeric term. Future work should focus on a scale-by-scale evaluation of each contributor to Eq. (15). Hopefully, this would allow to definitely assess the theory of drag reduction by Tabor & De Gennes (1986), which were the first to suggest an alteration of the energy cascade due to elasticity.

REFERENCES

Benzi, R. 2010 A short review on drag reduction by polymers in wall bounded turbulence. *Physica D* **239**, 1338–1345.

Carpenter, M. H. 1993 The stability of numerical boundary treatments for compact high-order finite-difference schemes. *J. Comp. Phys.* **108(2)**, 272–295.

De Gennes, P. G. 1986 Towards a scaling theory of drag reduction. *Physica D* **140**, 9–25.

Deville, M. O. & Gatski, T. B. 2012 *Mathematical Modeling for Complex Fluids and Flows*. Springer, Heidelberg.

Durbin, P. A. & Pettersson-Reif, B. A. 2010 *Statistical Theory and Modeling for Turbulent Flows*, 2nd edn. New York: John Wiley & Sons, Inc.

Housiadas, K. D. & Beris, A. N. 2003 Polymer-induced drag reduction: Effects of the variations in elasticity and inertia in turbulent viscoelastic channel flow. *Phys. Fluids.* **15**, 2369–2384.

Laufer, J. 1955 The structure of turbulence in fully developed pipe flow. *Tech. Rep.* 1174. Nat. Adv. Ctee Aero., Washington, USA.

Lele, S. K. 1992 Compact finite difference schemes with spectral-like resolution. *J. Comp. Phys.* **103(1)**, 16–42.

Lumley, J. L. 1969 Drag reduction by additives. *Annu. Rev. Fluid Mech.* **1(1)**, 367–384.

Morris, S. C. & Foss, J. F. 2005 Vorticity spectra in high reynolds number anisotropic turbulence. *Phys. Fluids* **17**, 088102/1–4.

Pope, S. B. 2000 *Turbulent Flows*. Cambridge, UK: Cambridge University Press.

Tabor, M. & De Gennes, P. G. 1986 A cascade theory of drag reduction. *Europhys. Lett.* **2**, 519–522.

Thais, L., Gatski, T. B. & Mompean, G. 2012 Some dynamical features of the turbulent flow of a viscoelastic fluid for reduced drag. *J. of Turbulence* **13**, 1–26.

Thais, L., Tejada-Martinez, A., Gatski, T. B. & Mompean, G. 2011 A massively parallel hybrid scheme for direct numerical simulation of turbulent viscoelastic channel flow. *Computers and Fluids* **43**, 134–142.

Virk, P. S. 1975 Drag reduction fundamentals. *AIChE* **21**, 625–656.

Warholic, M. D., Massah, J. & Hanratty, T. J. 1999 Influence of drag reducing polymers on turbulence: effects of Reynolds number, concentration and mixing. *Exps. Fluids.* **27**, 461–472.